Influence of Pearlite Formation on the Ductility Response of Commercial Hadfield Steel

M. Martín, M. Raposo, A. Druker, C. Sobrero & J. Malarría

Metallography, Microstructure, and Analysis
Application and Innovation for Metals, Alloys, and Engineered Materials

ISSN 2192-9262
Volume 5
Number 6

Metallogr. Microstruct. Anal. (2016) 5:505-511
DOI 10.1007/s13632-016-0316-7

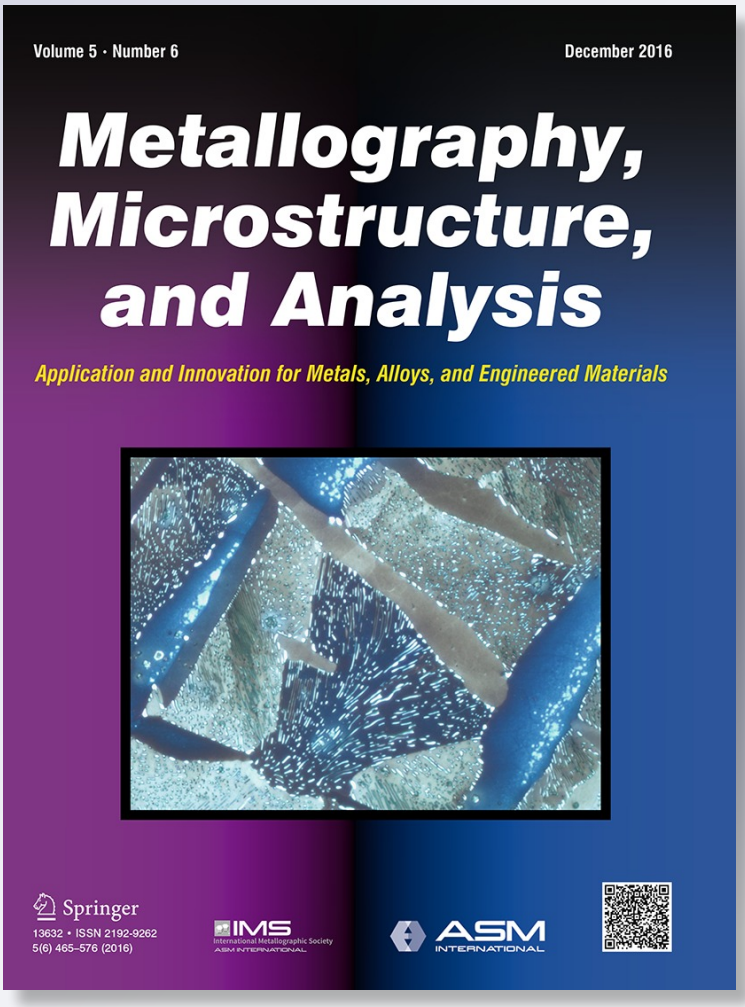

Springer

Metallogr. Microstruct. Anal. (2016) 5:505–511
DOI 10.1007/s13632-016-0316-7

TECHNICAL ARTICLE

Influence of Pearlite Formation on the Ductility Response of Commercial Hadfield Steel

M. Martín[1] · M. Raposo[1] · A. Druker[1] · C. Sobrero[1] · J. Malarría[1]

Received: 25 August 2016 / Revised: 13 October 2016 / Accepted: 14 October 2016 / Published online: 26 October 2016

Abstract This manuscript presents the singular event of pearlite occurrence in commercially produced Hadfield steel. A detailed characterization of the microstructure is performed, and its influence on the mechanical properties of the material is analyzed. The found microstructure may be interpreted as carbide formation if observed at the optical microscope. However, it consists of an extremely fine lamellae structure ranging from 40 to 130 nm of thickness. Experimental evidence of pearlite formation is supported by microhardness measurements, X-ray diffraction, and secondary electron microscopy. The pearlite is located on the austenitic grain boundaries and within by means of intragranular islands. The occurrence of this phase is detrimental for the ductility response of the material assessed by means of uniaxial tensile testing and reduction in area determination. It is observed that a pearlite fraction of 20% is responsible for a reduction of 90% in elongation at fracture and a drop of 80% in reduction in area. A short heat treatment performed at 1050 °C allows recovering the ductility response of the material keeping grain size and chemical composition unchanged.

Keywords Hadfield steel · Pearlite · Tensile deformation · Ductility loss · X-ray diffraction

✉ M. Martín
martin@ifir-conicet.gov.ar

[1] Institute of Physics Rosario CONICET-UNR, 27 de Febrero 210 bis, S2000EZP Rosario, Argentina

Introduction

The Hadfield manganese steel is an abrasion resistant alloy widely applied to industrial uses like hammer mills, crusher liners, railways, and mining. Because of the high industrial relevance of this alloy, there is a lack of detailed studies relating critical features of the microstructure and mechanical properties. While austenite and carbides are the usual present phases in this material, pearlite formation can also occur in the Fe–12Mn–1C system.

In a solution-annealed and quenched condition, the Hadfield steel possesses a fully austenitic microstructure [1]. The high carbon and manganese content in the alloy leads to a very stable austenite both thermodynamically and against strain-induced transformation [2]. The austenitic matrix is nonmagnetic and combines high ductility, high toughness, and high work hardening [1]. The rapid work hardening is the reason for the high wear resistance of the alloy. Two main mechanisms are responsible for work hardening in Hadfield steel: the activation of multiple twinning systems and the dynamic strain aging [3–6].

Depending on the thermomechanical processing, carbide formation can occur owing to the hypereutectoid character of the alloy [2, 7, 8]. Both the austenite and the carbides are the usual microstructural features found in Hadfield manganese steel.

At the moment, the available information about pearlite formation in Hadfield steels refers to specific studies of nucleation and growth under laboratory conditions. Such investigations comprise isothermal heat treatments with holding times lasting for several days which pursue the formation of thick lamellas intended for crystallographic studies [9–15]. In this case, we call the attention on a much finer microstructure occurring in the as-received condition of commercial material. This second phase may be

confused with carbide formation if observed at the optical microscope and results detrimental for the material's ductility. Accordingly, a detailed characterization is presented together with the proper heat treatment to revert the transformation and recover the ductility response of this type of steel.

Materials and Experimental Procedure

The material under study is commercial Hadfield manganese steel whose chemical composition is listed in Table 1. Steel sheets of 4 mm thickness were received for mechanical testing and qualification of the material. The sheets were provided by an industry partner who observed premature failures of the material during curving operations.

Mechanical properties were assessed by means of uniaxial tensile tests. To do that, tensile specimens were machined out of the steel sheets parallel to the rolling direction by means of wire electrical discharge machining. The specimen's geometry was defined according to ASTM E8 standard with a gauge length of 25 mm. Tensile tests were carried out until rupture with an initial strain rate of 3×10^{-4} 1/s according to mean values used in [2]. Three tests were performed for every material's condition. While yield strength and tensile strength were determined out of the tensile curves, the elongation at fracture and reduction in area were obtained ex situ by means of a digital caliper.

Samples for optical microscopy and X-ray diffraction were prepared out of the grip area of tested specimens. Transversal cross sections were cut, grinded, and polished up to 1 μm with diamond paste. Following, the samples were subjected to an electropolishing process employing a solution of acetic/perchloric acid in a 80/20 proportion. A 5% nital solution was employed to reveal the microstructure. Etched samples were observed at 10 kV and magnifications up to 60,000×.

Microhardness and grain size measurements were performed on transversal cross sections of the grip area as well. Values of Vickers hardness were obtained using a microhardness tester with an applied load of 100 g and duration of 15 s. A minimum of five measurements were performed in every phase. Grain size values were determined by the linear intercept method without considering twin boundaries.

The acquisition of the diffraction patterns was performed in the 35°–100° 2θ range with a Cu kα radiation, using a graphite monochromator.

Heat treatment was performed in a muffle-type furnace under flowing argon gas to reduce oxidation. The material was solution annealed at 1050 °C during 15 min followed by water quenching.

Results

Measuring the chemical composition by optical emission spectroscopy was the first step in order to qualify the material. The values obtained for carbon, silicon, and manganese content were in agreement with the standard specification for austenitic manganese steels ASTM A-128, as shown in Table 1. Following, the tensile properties of the as-received material were determined. As shown in Fig. 1, the engineering stress–strain curves of the as-received material are quite different from what expected for an austenitic steel. Specifically, they present a steep strain hardening during the plastic regime which finishes with an abrupt rupture and a very low macroscopic deformation. The poor ductility response of the as-received material is quantified by average values of elongation at fracture and reduction in area of 8 and 5%, respectively, as shown in Table 2.

Subsequently to the evaluation of the tensile behavior, the microstructure of the as-received material was examined. As presented in Fig. 2a, a secondary phase decorates the grain boundaries in allotriomorphs manner and forms islands within the grains too. Image analysis performed on the optical micrographs indicated a fraction area between 18 and 22% for the secondary phase. At the optical microscope, this phase has a "carbide-like" appearance. This observation and the presence of 0.1 wt% of chromium in the alloy, see Table 1, motivated the accomplishment of the microhardness measurements. The average hardness value obtained for the secondary phase was 370 HV 0.1 at both the islands and the grain boundary formations, as shown in Table 3. This magnitude is far below of the 1100 HV 0.1 reported for chromium carbides [16].

Table 1 Chemical composition of commercial Hadfield steel in wt%

Condition	C	Si	Mn	Cr	Fe
As-received	1.01	0.32	12.6	0.1	Bal.
Annealed (15 min—1050 °C)	1.00	0.33	12.7	0.1	Bal.
ASTM A 128, B-1 grade [20]	0.9–1.05	1.0 max.	11.5–14.0	–	Bal.

Measured by means of optical emission spectroscopy

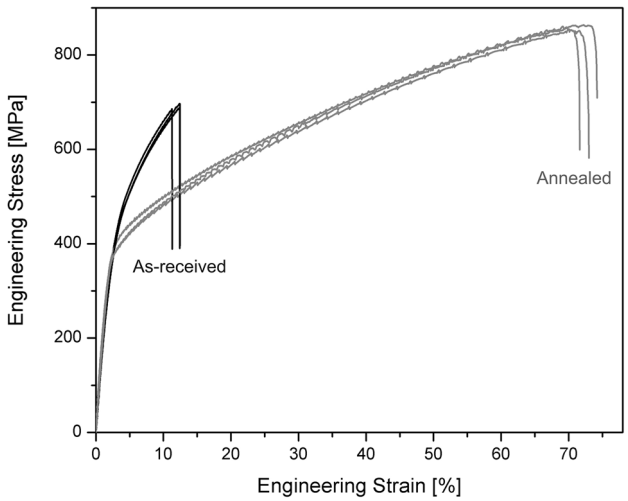

Fig. 1 Engineering stress–strain curves of commercially produced Hadfield steels in the as-received and annealed condition

Table 2 Mechanical properties of Hadfield steel obtained by tensile testing at room temperature

Condition	$Rp_{0.2}$ (MPa)	Rm (MPa)	E_f (%)	Z (%)
As-received	387	696	8	6
	385	686	7	4
	384	688	8	5
Annealed	364	854	67	28
	360	858	66	31
	365	863	68	29

$Rp_{0.2}$ 0.2% offset yield strength, *Rm* tensile strength, *E_f* elongation at fracture, *Z* reduction in area

Metallographic and hardness characterization was followed by X-ray diffraction analysis. Figure 3 presents the diffraction patterns of transversal cross section of tensile specimens (grip area). As can be seen, the as-received material is far away of being a single austenite phase. A body-centered cubic pattern was detected at the angular positions 45°, 65°, and 83° 2θ corresponding with the Fe-α reflections (110), (200), and (211). A third reflection set was detected between 30° and 50° 2θ in the alloy. This area is highlighted with a dashed box and enlarged in the upper right corner of Fig. 3. The comparison of such data with the results of several authors indicates the presence of orthorhombic cementite [17–19]. This type of cementite occurring in the Fe–C–Mn system is usually referred as M_3C with M representing the metallic atom iron and manganese [13, 14].

The microstructural characteristics of the secondary phase were revealed by means of high-magnification scanning electron micrographs. Such observations showed a very thin lamellar microstructure for the formations at grain boundaries and the islands within the austenitic grains. Both the allotriomorphic pearlite and the intragranular pearlite are internally formed by multiple colonies, as shown in Fig. 4. Three growth patterns were identified for the pearlite colonies: intragranular growth, as shown in Figs. 2a and 4a; preferential growth in one austenite grain, as shown in Fig. 4b; and growth in two adjacent grains, as shown in Fig. 4c. A detailed view of the thin lamellar structure is shown in Fig. 4d. The lamellae vary in thickness, can develop straightly, can accommodate curvature, and undergo branching. A lamellae thickness of

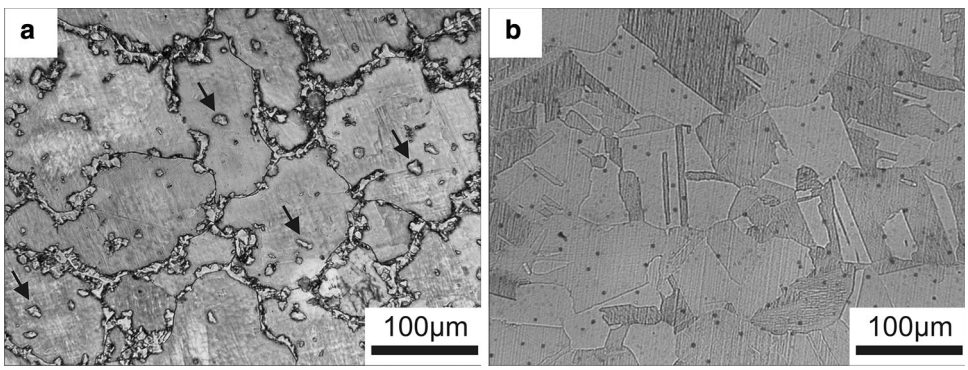

Fig. 2 Optical micrographs of Hadfield steels. **(a)** As-received material, arrows point to intragranular formations; (**b**) annealed material, 15 min at 1050 °C

Table 3 Mean values of Vickers microhardness and grain size

Condition	Phase	Microhardness HV 0.1	Mean grain size (μm/G-ASTM)
As-received	Secondary phase	372	98/3.5
	Matrix	280	
Annealed	Matrix	242	103/3.5

40–130 nm was determined by analyzing high-magnification micrographs like Fig. 4d.

The presence of pearlite as a secondary phase is the result of a diffusion process which creates a depletion of carbon and manganese in the austenitic matrix. Local variations in chemical composition plus the occurrence of a harder and more fragile phase in comparison with the austenitic matrix modify the mechanical properties of the material as shown in Fig. 1. To overcome this situation, a short solution annealing was chosen to achieve a single phase with a uniform carbon distribution and minimal grain size modification. The microstructure obtained after a solution annealing of 15 min at 1050 °C followed by water quenching is presented in Fig. 2b. The annealed microstructure features relatively thick thermal twins and a slight increase in grain size, as shown in Table 3. The complete austenitic character of the annealed material is confirmed by the X-ray diffraction pattern in Fig. 3. Such microstructure allows recovering the expected mechanical properties as depicted in Fig. 1. Of special interest are the new average values reached for elongation at fracture, E_f of 67%, and reduction in area, Z of 29%, presented in Table 2. The extended plastic regime of the annealed material allows visualizing the characteristic serrated flow of Hadfield steels. Such behavior is related to the hardening mechanisms occurring in this type of material during plastic deformation [2, 6].

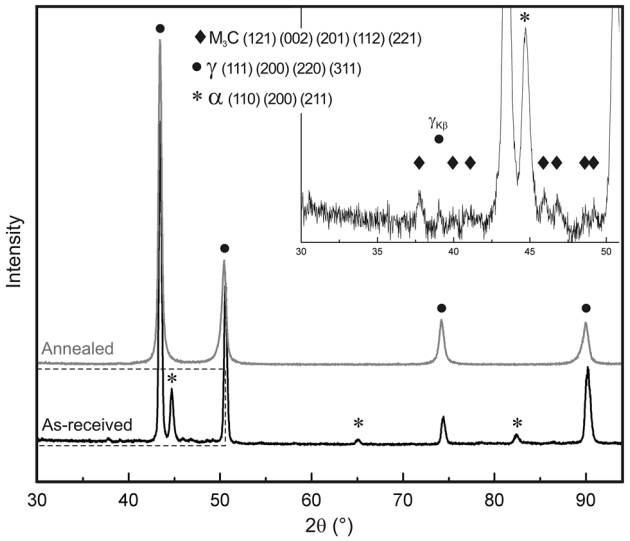

Fig. 3 X-ray diffraction patterns of Hadfield steels in as-received and annealed condition. The dashed box is magnified on the right upper corner

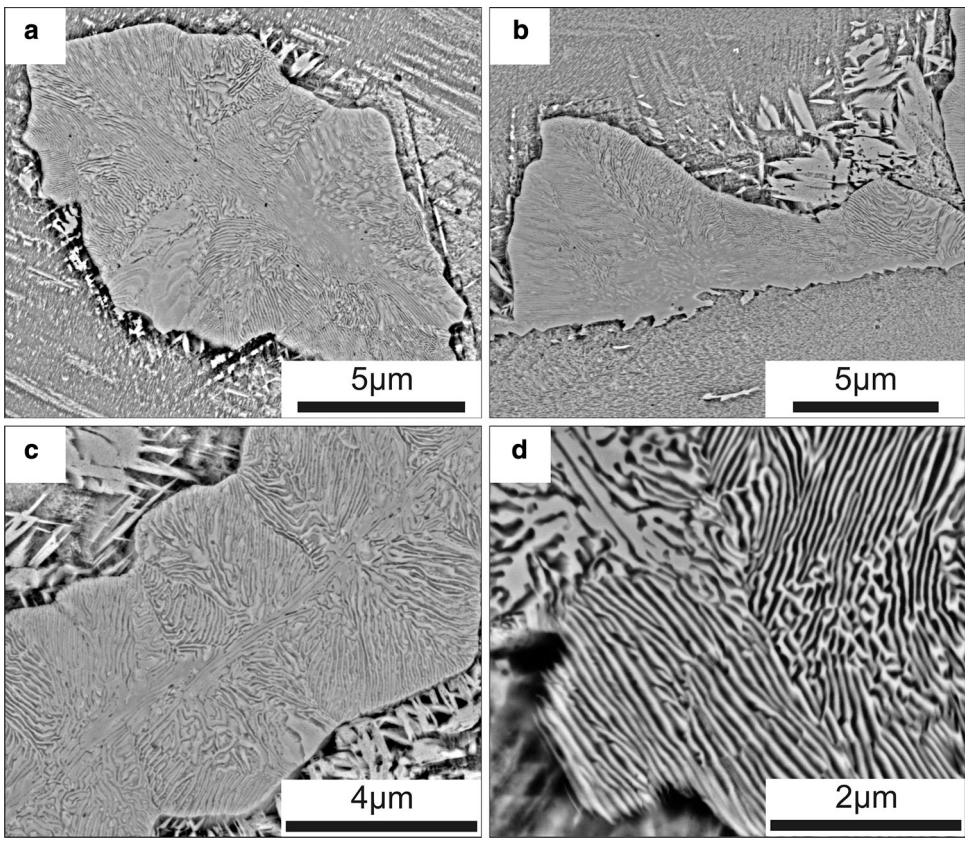

Fig. 4 Electron scanning micrographs of the as-received material. (**a**) Pearlite colony within an austenitic grain, pointed with arrows in Fig. 2a; (**b**) pearlite colony growing preferentially in one austenite grain; (**c**) pearlite colonies growing in two adjacent austenite grains; (**d**) detail of lamellar structure in pearlite colonies

Discussion

The as-received material can be qualified as a B-1 Hadfield steel grade according to its chemical composition and the corresponding standard [20]. Despite being in agreement with the specified composition, its mechanical performance is far away from a standard Fe–12Mn–1C alloy. Usually these alloys show a yield strength around 380 MPa, tensile strength about 960 MPa, and 50% of elongation [2]. Although the as-received material might fulfill the yield strength requirement, values of tensile strength, elongation at fracture, and reduction in area are too low for this type of alloy, as shown in Table 2. Such performance can be related to the secondary phase found in the as-received condition, as shown in Fig. 2b. As shown by hardness measurements, this phase does not correspond to the formation of chromium carbides. While the secondary phase posses a hardness value of 372 HV 0.1, as shown in Table 3, reported values for chromium carbides are about 1100 HV 0.1 [16]. Further analysis of X-ray diffraction patterns for the as-received material verified the absence of carbides and confirmed the presence of Fe-α and orthorhombic cementite, as shown in Fig. 3. These findings and the microstructure revealed by SEM micrographs in Fig. 4 prove the presence of pearlite in the as-received material. Since the presence of carbides in the as-received material was discarded by means of microhardness measurements and X-ray diffraction analysis, the pearlite is the only phase that gets dissolved during annealing. Therefore, the gain in ductility after heat treatment is due to the reversion of pearlite into austenite which also comprises the homogenization of local chemical composition by means of carbon and manganese redistribution.

The occurrence of pearlite in this type of alloy results out of a stepwise mechanism involving the precipitation of cementite and ferrite formation. The isoplethal section of the Fe–C–Mn system at 13% of manganese locates the eutectoid composition at 0.3% carbon content [18]. With 1% carbon content, the Hadfield steel is located to the right of the eutectoid composition and thermodynamic equilibrium indicates the presence of the two phase field austenite–cementite between 620 and 820 °C [13]. The cementite formed within this two phase field, known as proeutectoid cementite, is the first stage on the formation of pearlite colonies [9, 10, 15, 19, 21]. With the formation of a cementite nucleus, the surrounding austenite is depleted of carbon and the driving force for ferrite formation is increased [22]. Once a ferrite nucleus forms adjacent to the cementite nucleus, the process repeats itself and pearlite colony can grow stepwise by lateral movements [9, 10]. The size and shape of the proeutectoid cementite influence the growing pattern of the pearlite colony. A continuous layer of proeutectoid cementite along grain boundary gives rise to elongated colonies rather than hemispherical and promotes simultaneous growth in adjacent grains [15]. Such nucleation pattern was mostly found in as-received material as shown in Fig. 4b and c.

It was mentioned that in a solution-annealed and quenched condition the Hadfield steel possesses a fully austenitic microstructure [1]. This means that a wrong thermomechanical processing performed on the alloy is responsible for the occurrence of pearlite. In this regard, Dippenaar and Honeycombe reported the time–temperature–transformation curve for pearlite in Hadfield steel with the nose located at 550 °C [15]. In addition, they showed that 1 h isothermal heat treatment at 550 °C leads to a 15–20% of transformation with most pearlite nucleating at the austenitic grain boundaries. Comparing the results of Dippenaar–Honeycombe with the pearlite fraction, 18–22%, and the nucleation mode found in this work, we conclude that the material was subjected to a temperature close to 550 °C for ca. 1 h during production processing.

Investigations of pearlite nucleation in Hadfield steels at laboratory conditions report the occurrence of M_3C cementite and a main role of manganese partition in pearlite formation [13, 14, 23]. Ontman and Shiflet were able to image the element manganese within a coarse pearlite obtained after 14–90 days of isothermal heat treatment by means of SEM techniques [14]. Such conditioning resulted in lamellar widths of 1 μm to 2.5 μm versus the 40–130 nm found in this case, see Fig. 4. The very thin lamellar spacing in the as-received material made impossible to map the element manganese in the cementite. Nonetheless, energy-dispersive X-ray spectroscopy (EDS) measurements were performed in the austenitic matrix and the pearlite colonies at areas of 5 μm times 5 μm. Similar manganese contents were found in both phases as shown in Table 4. The presence of manganese in the pearlite and the complete solid solution of iron and manganese in cementite reported by Dierkes and Dronskowski suggest the occurrence of $Fe_{3-x}Mn_xC$ cementite in this case [17].

Tensile testing shows that the occurrence of pearlite decreases the ductility response of Hadfield steel. In this matter, the short heat treatment carried out on the material was effective in recovering this property. Remarkable is the

Table 4 Manganese content quantification by means of energy-dispersive X-ray spectroscopy in wt%

Condition	Phase	#1	#2	#3
As-received	Austenite	11.70	12.00	12.04
	Pearlite	11.48	11.65	11.57

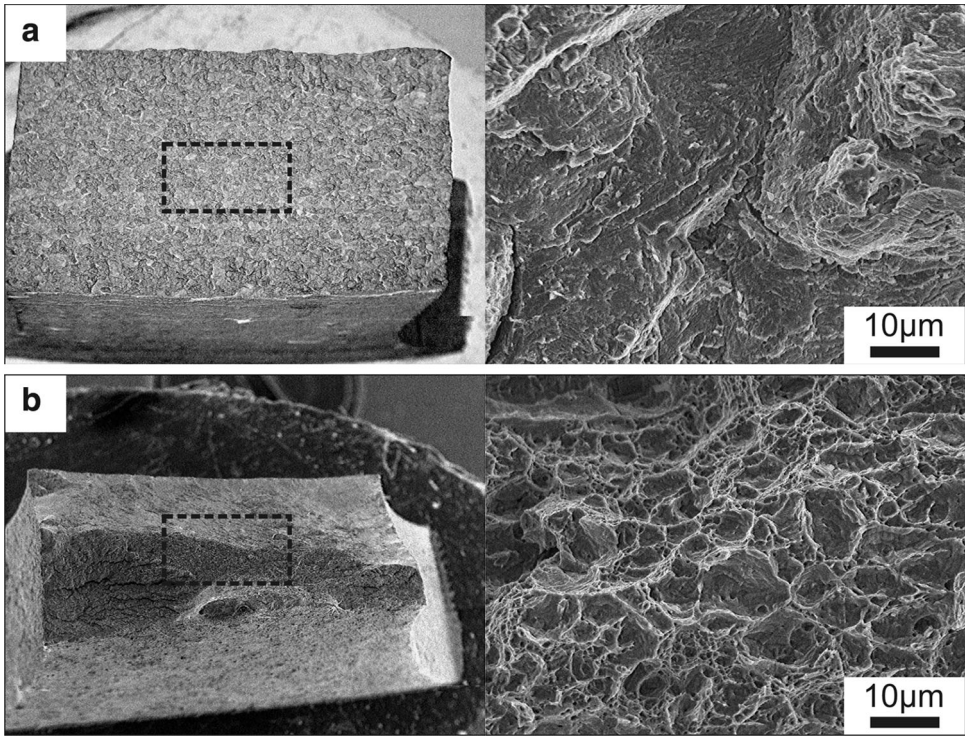

Fig. 5 Fracture surfaces of tensile specimens. (**a**) As-received material; (**b**) annealed material

gain on elongation at fracture and reduction in area by 9 and 6 times, respectively, as shown in Table 2. Fractographic observations are consistent with the mechanical assessment of ductility for both steel conditions. Figure 5 presents the fracture surface of tensile specimens by means of a macroscopic view and an enlarged image referring to the dashed box area. In there, a quasi-cleavage fracture is observed in the as-received condition, as shown in Fig. 5a, while a microvoid coalescence failure takes place in the annealed material, as shown in Fig. 5b. Both fracture surfaces are accompanied by a remarkable difference on macroscopic deformation, with a brittle transversal fracture in Fig. 5a and the presence of necking in the annealed condition, as shown in Fig. 5b.

The improvement on ductility occurs without decarburization and with a slight increase in grain size, as shown in Tables 1 and 3. On the other hand, a small drop of 20 MPa in yield strength and 40 HV 0.1 in hardness is registered for the annealed material, as shown in Tables 2 and 3. If needed, both properties could be easily increased by means of cold deformation.

Besides affecting ductility, the presence of pearlite is expected to harm the toughness of the material as well. Undesirable effects like the increase in ductile to brittle transition temperature and the reduction in absorbed impact energies with pearlite content have been reported in steels containing pearlite [24]. Such effects are related to the strength and brittleness of the lamellar cementite and the easiness of crack nucleation at the ferrite–cementite interfaces. Particularly, higher cementite plate thicknesses reduce the energy values in the upper shelf region of impact tests and increase the transition temperature [1, 24, 25]. The deleterious consequences of pearlite presence on the toughness of metallic materials include high manganese carbon steel, microalloyed steel, and ductile cast iron among others [26–29].

Conclusion

A singular microstructure occurring in commercial Hadfield steel is presented in detail. Although it may resemble to carbide precipitation through optical microscopy, microhardness measurements and X-ray diffraction confirm the presence of pearlite. The pearlite phase is located on the austenite grain boundaries and within the grains in form of islands. It is formed by a very thin lamellar structure of ferrite and cementite with thickness between 40 and 130 nm. Scanning electron micrographs evidenced three different growth patterns: intragranular growth, preferential growth in one austenite grain, and simultaneous growth in two adjacent grains. The manganese content measured on the pearlite colonies by means of EDS supports the occurrence of $Fe_{3-x}Mn_xC$ cementite.

A detected fraction of 20% of pearlite is responsible for a reduction of 90% in elongation at fracture and a drop of 80% in reduction in area. A short solution annealing performed at 1050 °C during 15 min allows recovering the

ductility response of the material. The improvement on ductility occurs without decarburization and with a slight increase in grain size.

Acknowledgments The authors acknowledge the support of CONICET (Argentina) under Grant PDTS-251.

References

1. H. Berns, W. Theisen, *Ferrous Materials—Steel and Cast Iron* (Springer, New York, 2008)
2. Y.N. Dastur, W.C. Leslie, Mechanism of work hardening in Hadfield manganese steel. Met. Trans. A **12**, 749 (1981)
3. I. Karaman, H. Sehitoglu, K. Gall, Y. Chumlyakov, H.J. Maier, Deformation of single crystal Hadfield steel by twinning and slip. Acta Mater. **48**, 1345 (2000)
4. P.H. Adler, G.B. Olson, W.S. Owen, Strain hardening of Hadfield manganese steel. Met. Mater. Trans. A **17**, 1725 (1986)
5. I. Karaman, H. Sehitoglu, K. Gall, Y.I. Chumlyakov, On the deformation mechanisms in single crystal Hadfield manganese steels. Scr. Mater. **38**, 1009 (1998)
6. W.S. Owen, M. Grujicic, Strain aging of austenitic Hadfield manganese steel. Acta Mater. **47**, 111 (1998)
7. D. Michalon, G. Mazet, C. Burgio, Manganese steel for abrasive environments. Tribol. Int. **9**, 171 (1976)
8. A. Goldberg, O. Ruano, O. Sherby, Development of ultrafine microstructures and superplasticity in Hadfield manganese steels. Mater. Sci. Eng. A **150**, 187 (1992)
9. S.A. Hackney, G.J. Shiflet, The pearlite-austenite growth interface in an Fe–0.8C–12Mn alloy. Acta Met. **35**, 1007 (1987)
10. S.A. Hackney, G.J. Shiflet, Pearlite growth mechanism. Acta Met. **35**, 1019 (1987)
11. S.A. Hackney, G.J. Shiflet, Interfacial structure at the pearlite: austenite growth interface in an Fe–0.8C–12Mn steel. Scr. Met. **19**, 757 (1985)
12. S.A. Hackney, Morphological instabilities and branching processes at the initiation of the eutectoid transformation. Scr. Met. Mater. **25**, 1453 (1991)
13. C.R. Hutchinson, G.J. Shiflet, The formation of partitioned pearlite at temperatures above the upper Ae1 in an Fe–C–Mn steel. Scr. Mater. **50**, 1 (2004)
14. A.Y.M. Ontman, G.J. Shiflet, Thermodynamic mapping of austenite decomposition's approach toward equilibrium in Fe–C–Mn at 700 °C. Acta Mater. **89**, 98 (2015)
15. R.J. Dippenaar, R.W.K. Honeycombe, The crystallography and nucleation of pearlite. Proc. R. Soc. A Math. Phys. Eng. Sci. **333**, 455 (1973)
16. M.M. Atabaki, S. Jafari, H. Abdollah-pour, Abrasive wear behavior of high chromium cast iron and Hadfield steel-A comparison. J. Iron. Steel Res. Int. **19**, 43 (2012)
17. H. Dierkes, R. Dronskowski, High-resolution powder neutron diffraction on Mn3C. Z. Anorg. Allg. Chem. **640**, 3148 (2014)
18. ASM International. Volume 3-Alloy Phase Diagrams (1992)
19. D.S. Zhou, G.J. Shiflet, Ferrite: cementite crystallography in pearlite. Met. Trans. A **23**, 1259 (1992)
20. ASTM A128/A128M - 93 Standard Specification for Steel Castings, Austenitic Manganese (2003)
21. M.X. Zhang, P.M. Kelly, The morphology and formation mechanism of pearlite in steels. Mater. Charact. **60**, 545 (2009)
22. D.A. Porter, K.E. Easterling, *Phase Transformations in Metals and Alloys* (Chapman & Hall, London, 1992)
23. N.A. Razik, G.W. Lorimer, N. Ridley, An investigation of manganese partitioning during the austenite-pearlite transformation using analytical electron microscopy. Acta Met. **22**, 1249 (1974)
24. A.R. Rosenfield, G.T. Hahn, J.D. Embury, Fracture of steels containing pearlite. Met. Trans. **3**, 2797 (1972)
25. H.K.D.H. Bhadeshia, R. Honeycombe, *Steels-Microstructure and Properties*, 3rd edn. (Butterworth-Heinemann, Oxford, 2006)
26. P.J.J. Ratto, A.F. Ansaldi, V.E. Fierro, F.R. Agüera, H.N. Alvarez, Villar, and J. A. Sikora, Low temperature impact tests in austempered ductile iron and other spheroidal graphite cast iron structures. ISIJ Int. **41**, 372 (2001)
27. H. Kim, M. Kang, H.J. Jung, H.S. Kim, C.M. Bae, S. Lee, Mechanisms of toughness improvement in Charpy impact and fracture toughness tests of non-heat-treating cold-drawn steel bar. Mater. Sci. Eng. A **571**, 38 (2013)
28. I. Gutiérrez, Effect of microstructure on the impact toughness of Nb-microalloyed steel: Generalisation of existing relations from ferrite-pearlite to high strength microstructures. Mater. Sci. Eng. A **571**, 57 (2013)
29. R.A. Gonzaga, Influence of ferrite and pearlite content on mechanical properties of ductile cast irons. Mater. Sci. Eng., A **567**, 1 (2013)